Clinical Anatomy 28:45–51 (2015)

ORIGINAL COMMUNICATION

Microsurgical Anatomy of the Posterior Median Septum of the Human Spinal Cord

ERHAN TURKOGLU,[1] HAYRI KERTMEN,[1] KUTLUAY ULUC,[1] ERINC AKTURE,[1] BORA GURER,[1] ULAŞ CIKLA,[1] SHAHRIAR SALAMAT,[2] AND MUSTAFA K. BAŞKAYA[1]*

[1]*Department of Neurological Surgery, School of Medicine and Public Health, University of Wisconsin, Madison, Wisconsin*

[2]*Department of Pathology and Laboratory, Medicine, School of Medicine and Public Health, University of Wisconsin, Madison, Wisconsin*

The aim of this study was to analyze the topographical anatomy of the dorsal spinal cord (SC) in relation to the posterior median septum (PMS). This included the course and variations in the PMS, and its relationship to and distance from other dorsal spinal landmarks. Microsurgical anatomy of the PMS was examined in 12 formalin-fixed adult cadaveric SCs. Surface landmarks such as the dorsal root entry zone (DREZ), the denticulate ligament, the architecture of the leptomeninges and pial vascular distribution were noted. The PMS was examined histologically in all spinal segments. The PMS extended most deeply at spinal segments C7 and S4. This was statistically significant for all spinal segments except C5. The PMS was shallowest at segments T4 and T6, where it was statistically significantly thinner than at any other segment. In 80% of the SCs, small blood vessels were identified that traveled in a rostrocaudal direction in the PMS. The longest distance between the PMS and the DREZ was at the C1–C4 vertebral levels and the shortest distance was at the S5 level. Prevention of deficits following a dorsal midline neurosurgical approach to deep-seated SC lesions requires careful identification of the midline of the cord. The PMS and septum define the midline on the dorsum of the SC and their accurate identification is essential for a safe midline surgical approach. In this anatomical study, we describe the surface anatomy of the dorsal SC and its relationship with the PMS, which can be used to determine a safe entry zone into the SC. Clin. Anat. 28:45–51, 2015.

Key words: anatomy; posterior median septum; safe entry zone; spinal cord; surface anatomy

INTRODUCTION

Macallister (1889) demonstrated that in cross-sections, the human spinal cord (SC) is bilaterally symmetrical with respect to a partial midline division formed by the anterior median fissure and a posterior midline separation that has been called the "posterior median septum" (PMS). The PMS separates the left and right posterior white funiculi/columns. Parkinson (1991) revealed that the reconfiguration and structure of the midline separation between posterior columns varied considerably. The anatomy of the PMS differs at different spinal segments (Parkinson, 1995; Constantini et al., 2000; Bozkurt et al., 2012). For intramedullary tumor (IMT) surgeries, neurosurgeons must be familiar with the anatomical features of the PMS, as it represents a safe entry zone to the SC (Perese and Fracasso, 1959; Kothbauer, 2003; Jacquesson et al.,

*Correspondence to: Mustafa K. Baskaya, Department of Neurological Surgery, University of Wisconsin Hospital & Clinics, CSC K4/828, 600 Highland Avenue, Madison, Wisconsin 53792, USA. E-mail: m.baskaya@neurosurgery.wisc.edu

Received 4 September 2014; Revised 26 October 2014; Accepted 28 October 2014

Published online 1 December 2014 in Wiley Online Library (wileyonlinelibrary.com). DOI: 10.1002/ca.22490

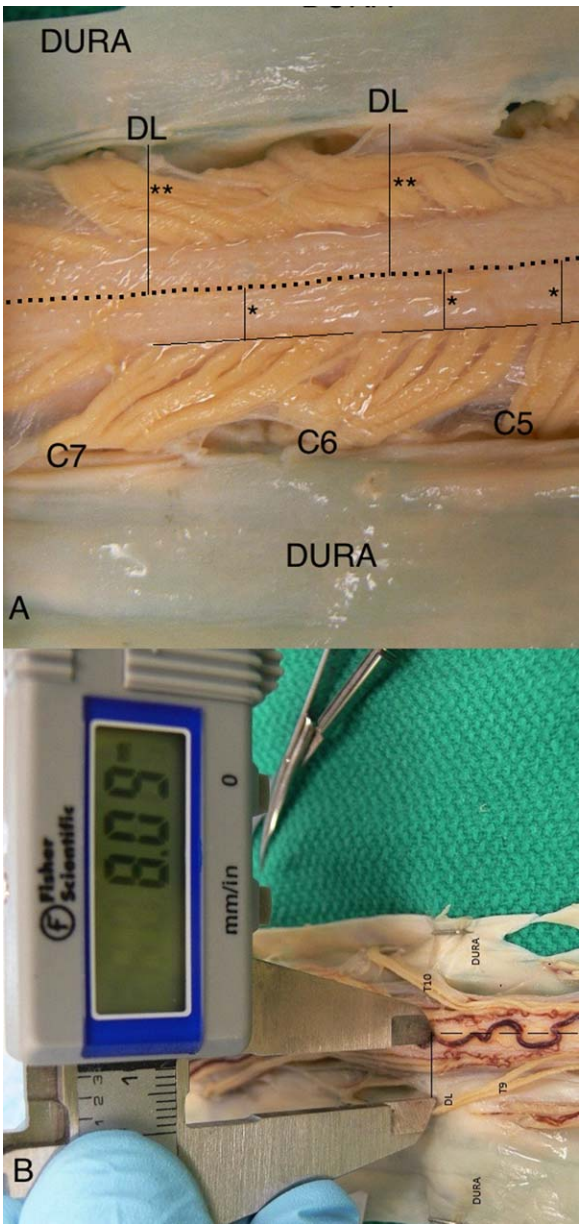

Fig. 1. (**a**) Macroscopic dorsal view of the cervical spinal cord at C6–8 segments showing the surface landmarks used in this study. Dashed lines represent the midline (PMS), solid lines represent the DREZ. The distances measured: *distance between the PMS and the DREZ (dorsal root entry zone), **distance between the PMS and the DL (denticulate ligament). (**b**) Measurement method with digital caliper employed in the study. Macroscopic dorsal view of the thoracic spinal cord at segments T9–T10. Solid line represents the distance measured from the midline to the denticulate ligament. Dashed line represents the midline and PMS. [Color figure can be viewed in the online issue, which is available at wileyonlinelibrary.com.].

2014). Successful determination and dissection of the PMS requires a comprehensive knowledge of its microsurgical anatomy and its relationship with other surface landmarks of the dorsal SC. However, there have been no quantitative studies of the length, thickness, depth, and configuration of the PMC and various surface landmarks of the SC other than that by Jacquesson et al. (2014).

The purpose of this study is to examine and illustrate the microanatomical features of the PMS and the associated surface landmarks comprehensively. This should improve the microneurosurgical approach during IMT surgery. We also discuss the anatomical terminology used for the PMS.

MATERIALS AND METHODS

The microsurgical anatomy of the PMS and associated surface landmarks were examined in 12 formalin-fixed adult cadaveric SCs. Of these samples, four (33%) were female cadavers and eight (67%) were male. The cadavers ranged from 42 to 81 (mean 62.5 ± 10.6) years of age. Exclusion criteria included traumatic or nontraumatic SC pathology, vertebral deformity, history of any neurological signs and symptoms related to the SC and/or the spinal nerves.

For each case a bilateral longitudinal laminectomy extending from C1 to S5 was performed using an autopsy saw (Stryker Instruments, Kalamazoo, MI) and the 12 thoracic ribs were exposed through a dorsal approach. Once the SC was exposed, the limits of the thoracic cord were confirmed by matching the thoracic nerve roots with their corresponding ribs. The cervical, lumbar and sacral segments were subsequently identified by counting the remaining roots cranially and caudally. Upon extraction, the entire SC was removed en bloc and allowed to fix in 10% buffered formalin for 14 days. Following fixation, the dura and arachnoid were opened using microsurgical instruments and fixed with silk sutures to a dissecting board. Durotomy extending from the cranial to the caudal end was performed to expose the entire length of the SC. Orthogonal transverse sections were obtained with razor blades at the cervical, thoracic and lumbar regions, corresponding to the nerve root exits. For each major SC region, the total length, individual segment lengths and width were recorded. All measurements were obtained directly from the fixed tissue using Fisher Traceable Digital Calipers (Fisher Scientific, Pittsburgh, PA; Fig. 1).

The dorsal surface of the SC was examined to determine the precise location of the midline. Several surface landmarks were used to identify the optimal location for the PMS: the denticulate ligament (DL), the dorsal root entry zone (DREZ), the architecture of the leptomeninges and pial vascular distribution (Figs. 2a–2e). Microsurgical examination and measurements of the PMS and the associated surface landmarks were performed under a surgical microscope (Leica Wild M 695, Leica Microsystems Inc., Wetzlar, Germany) at magnifications of 2–40×. Photographs were taken during the examination with an operating microscope using Medx Change software (MEDX Inc., Arlington Heights, IL) integrated with the surgical microscope. The meninges and posterior median sulcus were dissected under the surgical microscope using microscissors, microtweezers, and microspatulas. During

dissection, particular attention was given to preserving the arachnoid and pia layers with accompanying blood vessels. Depending on the spinal segments, the PMS was obscured by venous channels that required lateral displacement in order to expose the sulcus. As a next step, the pia was incised midline-longitudinally, spontaneously separating the gracil fasciculi at the midline. The dissection was extended deep between the gracil fasciculi toward the central canal. Small vascular channels were observed along the septum. Following dissection, all SCs were sectioned into cervical, thoracic, lumbar and sacral regions comprising eight, twelve, five and five segments, respectively. For each segment, the following data were recorded bilaterally: distance between the PMS and DL, distance between the PMS and DREZ.

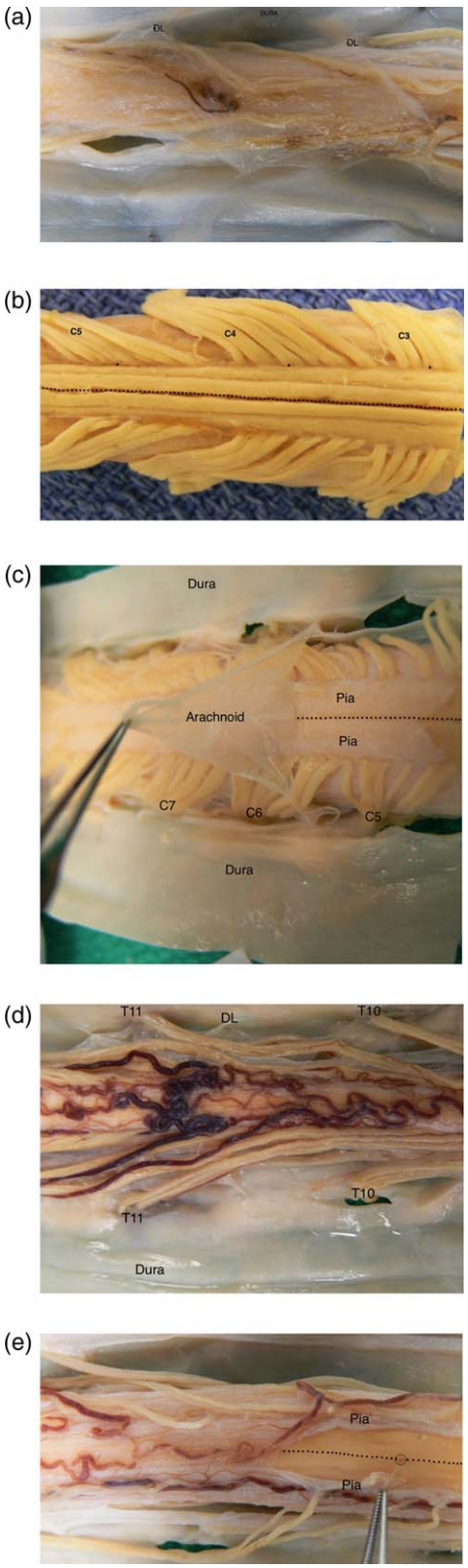

Light Microscopic Examination

For each SC segment a 3–4-mm thick transverse section was taken and subjected to routine processing and paraffin embedding. Five-μm thick sections of paraffin-embedded tissues were stained with hematoxylin and eosin (H&E). The stained tissue sections were examined using an Olympus BH2 microscope (Olympus Optical Company, Japan) and photographs were taken using Phantomatic-X film 100 with an Olympus camera. The PMS depth was measured in tissue sections for all segments and recorded in mm using light microscopic scales. The shape and extent of PMS were investigated and categorized in a manner similar to that reported by Parkinson and Delbigio (1996).

Statistical Analysis

Data were analyzed using SPSS for Windows version 11. 5 (SPSS Inc., Chicago, IL). Descriptive statistics (mean, median, standard deviation, frequency, minimum, maximum, and range) for all variables in our study were calculated. The Mann–Whitney *U* test was used for statistical assessment of differences in SC lengths and for the lengths of the cervical, thoracic, lumbar and sacral regions according to sex. Simple repeated measures analysis of variance was used for differences between the measurements from each cervical, thoracic, lumbar and sacral segment. The least squares difference post hoc test was performed when the significance reached $P < 0.001$.

Fig. 2. (**a**) Macroscopic dorsal view of the cadaveric thoracic spinal cord at vertebrae T7–T8 shows that the pia mater of the spinal cord has a pair of denticulate ligaments (one on each side of the spinal cord); DL; denticulate ligament. (**b**) Macroscopic dorsal view of the cadaveric cervical spinal cord at vertebrae C3-C5 shows the dorsal root entry zones (*). Dashed lines represent the midline. (**c**) Macroscopic dorsal view of the cadaveric cervical spinal cord at vertebrae C5–C7 shows the arachnoid mater attached to the PMS at the midline (solid line) and piamater. (**d**) Macroscopic dorsal view of the cadaveric cervical spinal cord at vertebrae T10–11 shows the longitudinal array of the pial vessels that indicates the midline. (**e**) After dissection of the arachnoid and the piamaters using microsurgical techniques, multiple tiny vessels (circle) coming from the surface and going deeply along the PMS indicate the midline. [Color figure can be viewed in the online issue, which is available at wileyonlinelibrary.com.]

TABLE 1. Sex Analysis Related to SCL, CeRL, TRL, LRL, and SaRL, in cm

	Female ($n = 4$)				Male ($n = 8$)				Total ($n = 12$)				
	Mean	Std. deviation	Median	Range	Mean	Std. deviation	Median	Range	Mean	Std. deviation	Median	Range	*P* value
SCL	43.25	8.26	42.50	18.00	42.33	3.77	42.50	12.00	42.56	4.91	42.50	18.00	0.953
CeRL	8.25	2.36	9.00	5.00	9.92	2.32	10.50	7.00	9.50	2.37	10.00	8.00	0.262
TRL	22.00	1.68	21.25	3.50	22.33	1.97	22.50	6.00	22.25	1.85	22.00	6.00	0.862
LRL	5.38	0.48	5.25	1.00	5.21	0.50	5.00	1.50	5.25	0.48	5.00	1.50	0.521
SaRL	3.38	0.25	3.50	0.50	3.50	0.56	3.25	1.50	3.47	0.50	3.50	1.50	0.862

CeRL, cervical region length; LRL, lumbar region length; SCL, spinal cord length; SaRL, sacral region length; Std, standard; TRL, thoracal region length.

Pearson's correlation test was used to examine the correlation between the mean values of the measurements of the transverse diameters, the DREZs, the PMS and the dentaticulate ligament of each segment. Statistical significance was set at $P < 0.001$.

RESULTS

Length and Width of Spinal Segments

The average length of all SCs examined was 42.6 ± 4.9 cm with a range of 35–53 cm. All SCs had 8 cervical, 12 thoracic, 5 lumbar, and 6 sacrococcygeal segments.

The cervical, thoracic, lumbar and sacral segments comprised 25.5, 53.4, 13.6, and 7.5% of the entire length of the SC, respectively. The longest SC segment was at T7. The lengths of the coccyx segments were added to the length of the last sacral segment. There was no significant sex difference in total cord length or the lengths of the cervical, thoracic and sacral regions ($P > 0.001$; Table 1). The SC was widest at the cervical segments followed by the thoracic, lumbar, and sacral segments. The widest cord segment was at C6 with a mean diameter of 13.5 ± 0.74 mm (11.7–14.6 mm). The mid-thoracic cord mean diameter was 9.6 ± 0.78 mm (8.4–11.2 mm) and the lumbar enlargement was observed at L3 with a mean

TABLE 2. Measurements From Surface Landmarks to the Posterior Median Septum in 12 Adult Spinal Cords

Segment	TD, mm ± SD	Depth of PMS, mm ±SD	DREZ, mm ± SD	DL, mm ± SD
C1	10.69 ± 0.67	0.14 ± 0.06	3.01 ± 0.40	12.76 ± 0.89
C2	11.62 ± 0.68	0.24 ± 0.12	3.15 ± 0.40	12.50 ± 0.91
C3	12.11 ± 0.70	0.21 ± 0.09	3.08 ± 0.42	11.88 ± 1.10
C4	12.52 ± 0.79	0.29 ± 0.15	3.18 ± 0.40	10.81 ± 1.35
C5	12.69 ± 1.04	0.22 ± 0.16	2.96 ± 0.41	10.90 ± 1.21
C6	13.49 ± 0.74	0.28 ± 0.16	2.87 ± 0.51	10.68 ± 1.19
C7	12.76 ± 1.43	0.46 ± 0.45	2.82 ± 0.49	10.86 ± 0.92
C8	12.36 ± 1.04	0.26 ± 0.15	2.63 ± 0.42	10.44 ± 1.12
T1	11.46 ± 1.16	0.19 ± 0.13	2.20 ± 0.42	9.66 ± 0.83
T2	10.83 ± 1.19	0.14 ± 0.07	2.17 ± 0.24	9.37 ± 0.63
T3	10.45 ± 1.01	0.14 ± 0.05	2.19 ± 0.26	9.21 ± 0.69
T4	10.23 ± 1.01	0.11 ± 0.03	2.28 ± 0.29	9.13 ± 0.55
T5	9.78 ± 0.93	0.17 ± 0.11	2.15 ± 0.26	8.78 ± 0.71
T6	9.60 ± 0.78	0.13 ± 0.06	2.36 ± 0.26	8.32 ± 0.74
T7	9.15 ± 0.81	0.14 ± 0.10	2.09 ± 0.20	8.64 ± 0.56
T8	8.94 ± 0.66	0.14 ± 0.07	2.12 ± 0.29	8.84 ± 0.51
T9	8.77 ± 0.55	0.18 ± 0.13	2.25 ± 0.38	8.80 ± 0.38
T10	8.59 ± 0.55	0.15 ± 0.09	2.29 ± 0.29	8.98 ± 0.45
T11	8.58 ± 0.62	0.19 ± 0.14	2.27 ± 0.19	9.05 ± 0.59
T12	8.39 ± 0.64	0.21 ± 0.13	2.28 ± 0.24	9.32 ± 0.98
L1	8.31 ± 0.52	0.18 ± 0.09	2.36 ± 0.32	9.14 ± 0.85
L2	8.52 ± 0.57	0.19 ± 0.10	2.20 ± 0.24	
L3	9.64 ± 0.66	0.25 ± 0.12	2.49 ± 0.33	
L4	8.81 ± 0.59	0.26 ± 0.05	2.24 ± 0.27	
L5	7.81 ± 0.85	0.27 ± 0.12	2.02 ± 0.25	
S1	7.03 ± 0.76	0.31 ± 0.15	1.79 ± 0.24	
S2	6.51 ± 0.93	0.30 ± 0.14	1.59 ± 0.29	
S3	6.05 ± 1.05	0.31 ± 0.13	1.41 ± 0.26	
S4	5.46 ± 1.26	0.35 ± 0.17	1.27 ± 0.22	
S5	4.61 ± 1.27	0.33 ± 0.17	1.14 ± 0.19	

DL, denticulate ligament; DREZ, dorsal root entry zone; PMS, posterior median septum; SD, standard deviation; TD, transverse diameter.

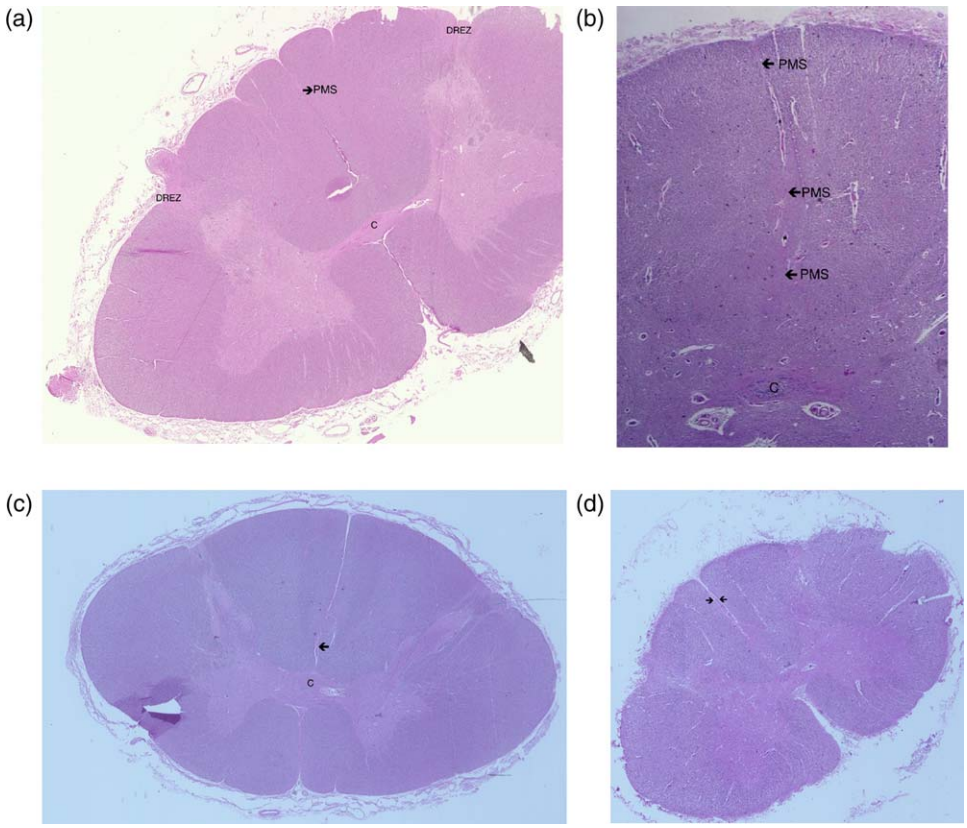

Fig. 3. (**a**) H&E staining of the spinal cord at vertebra C5 shows the classic, centered, straight and complete (from commissure to piamater) form of the PMS (arrow). C, commissure; DREZ, dorsal root entry zone; PMS, posterior median septum. (**b**) H&E staining of the spinal cord at vertebra T12 shows a missing part configuration of the PMS (*) from commissure to piamater. Magnification 2× (arrows; remaining part of the PMS). PMS, posterior median septum. (**c**) H&E staining of the spinal cord at vertebra C1 shows a gently curved line from the midline, which becomes straight thereafter (arrow). (**d**) H&E staining of the spinal cord at vertebra C2 and the reverse colored photograph in the lower left corner show a PMS that is forked and divided into two sections (arrows). C, commissure. [Color figure can be viewed in the online issue, which is available at wileyonlinelibrary.com.]

diameter of 9.6 ± 0.66 mm (8.5–10.8 mm; $P < 0.001$; Table 2).

Posterior Median Septum

The mean, range, and SD for each measurement obtained by light microscopy are presented in Table 2. The septum in the PMS was consistent throughout the SC, and while less evident in the thoracic segments it was more evident in the cervical, lumbar and sacral segments. The PMS was deepest at segments C7 and S4 segments with mean values of 0.46 ± 0.45 mm (0.1–2 mm) and 0.35 ± 0.17 mm (0.1–0.8 mm), respectively. In segments immediately adjacent to C7 and S4 the PMS was statistically significantly deeper than in other segments except for C5 (0.22 ± 0.16 mm; $P < 0.001$ for both comparisons). The PMS was shallowest at segments T4 and T6 with mean values of 0.11 ± 0.03 mm (0.1–0.2 mm) and 0.13 ± 0.06 mm (0.1–0.3 mm), respectively. In segments adjacent to T4 and T6 the PMS was statistically significantly shallower than in any other segment ($P < 0.001$). In most cases a PMS extended from the pial surface toward the posterior gray commissure. Like Parkinson and Delbigio (1996), we identified the following six variants: classic Type 1, which was straight, centered, complete and extended from the pial surface to the gray commissure; Type 2, which had missing portions/was fenestrated; Type 3, which was completely missing; Type 4, which had a single curve or multiple curves; Type 5, which was split, consisting of one or more components; and Type 6, which was incomplete and did not reach the gray commissure (Figs. 3a–3d). Ninety percent of the PMS configurations were Type 1 and the remaining 10% were classified as other types; no Type 7 configurations were observed in our study.

The arachnoid covered the entire SC and posterior surface vessels. The two dorsal spinal arteries sent small perforating branches laterally and medially. Small vascular branches penetrated the sulcus, separating the dorsal funiculi, even when the PMS was not distinctly present as a connective tissue

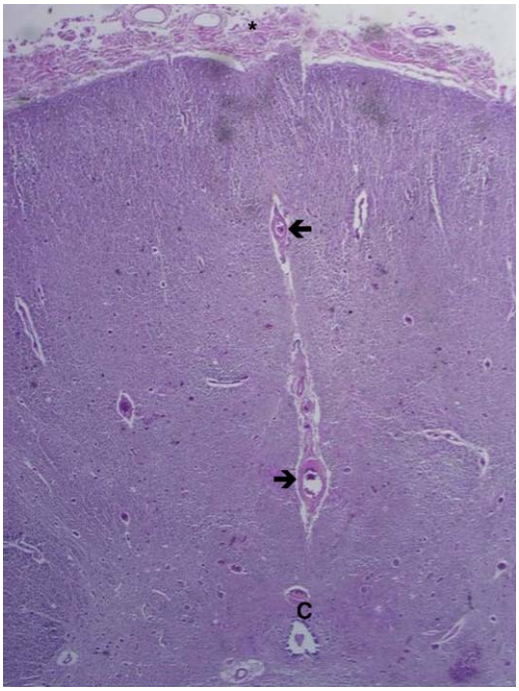

Fig. 4. H&E staining of the spinal cord at vertebra T9 shows the PMS (arrows) occupied by blood vessels from a part of the surface to the commissure. C, commissure, * posterior surface of the spinal cord. [Color figure can be viewed in the online issue, which is available at wileyonlinelibrary.com.]

layer. Additionally, small vascular channels traveled longitudinally along the PMS in 80% of the SCs (Fig. 4).

Distance from the Midline to Surface Landmarks

The mean, range and SD for each measurement are presented in Table 2. The DREZ was symmetrically positioned in relation to the midline on the dorsal surface of the SC. The longest distance between the PMS and the DREZ was at segment C4 with a mean value of 3.18 ± 0.36 mm (2.4–4 mm), and the shortest distance between the PMS and the DREZ occurred at segment S5 with a mean value of 1.14 ± 0.19 mm (1–1.7 mm). When these two segments (C4 and S5) were compared with others, the differences were statistically significant ($P < 0.001$). The DL was stretched between the lateral columns and the dura. Twenty-one pairs of DLs were observed in all SCs, attaching the cord laterally to the dura mater on each side (Fig. 2a). The longest distance between the PMS and the DL was at segment C1 with a mean value of 12.8 ± 0.89 mm (10.9–13.7 mm), and the shortest was at segment T6 with a mean value of 8.3 ± 0.74 mm (6.6–9.2 mm). The distance between the PMS and the DL was generally longer in the cervical segments and diminished caudally. When measurements at C1 and T6 were compared with others, the differences were statistically significant ($P < 0.001$).

DISCUSSION

The PMS is located in the midline and consists of a thin sheet of pia/arachnoid that extends from the dorsal surface toward the gray commissure of the SC and separates the dorsal funiculi on the left and the right (Key and Retzius, 1876; Elliott, 1945; Barson and Sands, 1977; Weller, 2005). Key and Retzius (1876) first reported the detailed anatomy of the dorsal spinal meninges and several authors have described this midline structure as "the septum arachnoidale," "septum intermedium," "septum leptomeningeum dorsale," or "median raphe" (Jacquesson et al., 2014; Parkinson and Delbigio, 1996; Weller, 2005). Studies by Samii and Keklamp (2007) revealed that the PMS extends from the cervical to the lumbar segments along the posterior midline and attaches to the pia. On the other hand, Jacquesson et al. (2014) could not identify a true septum in the PMS and described many small fibrous bridges "extending" the two dorsal columns. The PMS can reliably be used as a landmark during surgeries of SC tumors. Study by Brotchi (2002) stated that variously-sized vessels running medially on the posterior surface of the SC must be dissected and mobilized laterally to expose the posterior sulcus and septum, with attempts to spare all of the thinnest arterial or venous channels in the sulcocommissural region.

Our macroscopic, microdissection and histological observations suggest that the surgical approach has to be made precisely through the PMS, and gentle separation of the dorsal columns is vital for sparing the white matter and nerve functions. Elliott (1945) described the careful retraction and progressive opening of the dorsal columns over the entire length of the solid portion of the tumor. Detailed knowledge of dorsal surface landmarks in relation to the PMS is essential for the surgical planning of midline myelotomies. For a successful posterior midline myelotomy, optimal neuroanatomical orientation and precise microsurgical dissection are required. The most common indication for posterior midline myelotomy is intramedullary SC tumors (Angevine and McCormick, 2003; Sanderson and Cooper, 2003). However, since intramedullary lesions can divert or obscure the midline, their precise identification can become challenging. To achieve this critical step, identification of the right and left dorsal nerve rootlets and the DREZ can help to pinpoint the midline and the PMS (Bozkurt et al., 2012; Elliott, 1945; Fischer et al., 2005). Although the external and cross-sectional landmarks of the human SC have been well documented, there is very little information in the literature concerning the microsurgical anatomy of the PMS in adult human SCs (Lassek and Rasmussen, 1938; Sala et al., 2007; Bozkurt et al., 2012). To our knowledge, there are no published data on the quantitative measurement of the posterior surface anatomy of the SC with respect to the PMS and related surface landmarks.

The distances between the PMS and the associated surface landmarks have not been examined previously for each SC segment. Our results reveal that the distance between the PMS and the DREZ decreases progressively from a maximum 4 mm at segment C- to a

minimum of 1 mm at S- (mean 3.075–1.22 mm). The DLs anchor the cord to the dura mater and stabilize the SC against motion within the vertebral column (Weller, 2005). The distance between the PMS and the DL ranges from a maximum of 13.7 mm at the cervical segments (10.44 ± 1.12–12.76 ± 0.89) to a minimum of 6.6 mm at L1 (mean 12.76–8.32 mm). Herren and Alexander (1939) revealed that the vascular pattern on the dorsal surface of the SC can assist further with surgical planning for myelotomies, as branches from these vessels, which are mostly veins, travel with the PMS. In 80% of the SCs in our study there were small branches bridging between the pial venous channels on the dorsal SC and the small longitudinal vessels that travel with the PMS in a craniocaudal direction. Angevine and McCormick (2003) demonstrated that the accompanying vascular channels are quite valuable for orientation during dissection of the PMS. For a better functional outcome, longitudinal pial vessels that overlie the PMS or run close to it should be mobilized and preserved; however, small crossing vessels can be taken.

Like Jacquesson et al. (2014), we found the anterior white commissure was damaged in some samples during dissection of PMS, and the dissection extended beyond the central canal, reaching the anterior median sulcus. This is attributable to anatomical variations in the PMS. Parkinson and Delbigio (1996) reported eight types of PMS configuration. Type I: the classic septum that is centered, straight, and complete extending from the pia to the gray commissure; Type II: the septum is partially missing; Type III: the septum is completely missing; Type IV: the septum has a single curve; Type V: the septum has multiple curves with long or short wave lengths; Type VI: the septum arises off center; and Type VII: the septum is forked and/or divided into one or more components. In our study, we identified Types I, II, III, IV, V, VI, and VII PMS configurations. Parkinson and Delbigio (1996) found that ninety percent of the cases were Type I, whereas the remaining 10% of the cases were other types. In our study, the dorsal columns approximated to the midline in the all of the SCs and we saw no Type VII.

In conclusion, we identified several surface landmarks that can be used to identify the precise location of the posterior midline of the human SC. We believe that a combination of technological advances such as the operating microscope, intraoperative neurophysiological monitoring and microsurgical surface landmarks such as those identified in our study can help neurosurgeons to maintain their goal of maximizing tumor resection and minimizing neurological morbidity. Familiarization with the microanatomy of the PMS in the human SC is crucial for a surgical approach to intramedullary SC tumors. In less than 10% of cases, there is no distinct tissue layer that can be called a PMS. In such cases only small longitudinal blood vessels can be seen dividing the left and the right dorsal funiculi. Parkinson and Delbigio (1996) preferred to identify this dorsal median separation as "raphae."

ACKNOWLEDGMENTS

The authors would like to thank the donors of the cadavers used in this study.

REFERENCES

Angevine PD, McCormick PC. 2003. Spinal cord ependymomas. Operat Tech Neurosurg 6:9–14.

Barson AJ, Sands J. 1977. Regional and segmental characteristics of the human adult spinal cord. J Anat 123:797–803.

Bozkurt M, Canbay S, Neves GF, Aktüre E, Fidan E, Salamat MS, Başkaya MK. 2012. Microsurgical anatomy of the dorsal thoracic rootlets and dorsal root entry zones. Acta Neurochir (Wien) 154: 1235–1239.

Brotchi J. 2002. Intrinsic spinal cord tumor resection. Neurosurgery 50:1059–1063.

Constantini S, Miller DC, Allen JC, Rorke LB, Freed D, Epstein FJ. 2000. Radical excision of intramedullary spinal cord tumors: Surgical morbidity and long-term follow-up evaluation in 164 children and young adults. J Neurosurg 93:183–193.

Elliott KA. 1945. Cross-sectional diameters and areas of the human spinal cord. Anat Rec 93:287–293.

Fischer G, Brotchi J, Mahla K. 2005. Surgical management of intramedullary spinal cord tumors in adults. In: Schmidek H, Roberts D, editors. Schmidek and Sweet Operative Neurosurgical Techniques: Indications, Methods, and Results. Philadelphia: Saunders Elsevier. p 1945–1954.

Herren RY, Alexander L. 1939. Sulcal and intrinsic blood vessels of the human spinal cord. Arch Neurol Psychiatry 41:678–687.

Jacquesson T, Streichenberger N, Sindou M, Mertens P, Simon E. 2014. What is the dorsal median sulcus of the spinal cord? Interest for surgical approach of intramedullary tumors. Surg Radiol Anat 36:345–351.

Key EAH, Retzius MG. 1876. Srudien der Anatomie des Nervesystems und des Bindegewebes. Stockholm: Stockholm Samson Wallin.

Kothbauer KF. 2003. Intraoperative neurophysiologic monitoring for intramedullary spinal cord tumor surgery. Operat Tech Neurosurg 6:2–8.

Lassek AM, Rasmussen GL. 1938. A quantitative study of the newborn and adult spinal cords of man. J Comp Neurol 69: 371–379.

Macallister A. 1889. Text Book of Human Anatomy. 1st Ed. Philedelhia: P. Blakisten & Son and Co. p 7–745.

Parkinson D. 1991. Human arachnoid septa, trabecular, and "rogue strands." Am J Anat 192:498–539.

Parkinson D. 1995. Posterior septum of spinal cord: Normal developmental variations. FASEB J 9:1249.

Parkinson D, Delbigio MR. 1996. Posterior septum of human spinal cord: Normal developmental variations, composition, and terminology. Anat Rec 244:572–578.

Perese DM, Fracasso JE. 1959. Anatomical considerations in surgery of the spinal cord: A study of vessels and measurements of the cord. J Neurosurg 16:314–325.

Sala F, Bricolo A, Faccioli F, Lanteri P, Gerosa M. 2007. Surgery for intramedullary spinal cord tumors: The role of intraoperative (neurophysiological) monitoring. Eur Spine J 16:130–139.

Samii M, Keklamp J. 2007. Surgery of Spinal Tumors. Baltimore: Springer. p 526.

Sanderson SP, Cooper PR. 2003. Intramedullary spinal cord astrycytomas. Operat Tech Neurosurg 6:15–23.

Weller RO. 2005. Microscopic morphology and histology of the human meninges. Morphologie 89:22–34.